Article:
Yakub, I. and McGregor, J. (2022) Catalytic reduction of nitric oxide with hydrogen using carbon-supported d-metal catalysts. Waste and Biomass Valorization, 13 (3). pp. 1665-1680. ISSN: 1877-2641

https://doi.org/10.1007/s12649-021-01623-7

Catalytic Reduction of Nitric Oxide with Hydrogen using Carbon-supported *d*-metal Catalysts

Ibrahim Yakub[a,b] and James McGregor[a]

[a] Department of Chemical and Biological Engineering, University of Sheffield

[b] Department of Chemical Engineering and Energy Sustainability, Universiti Malaysia Sarawak

Corresponding author: Ibrahim Yakub. Department of Chemical Engineering and Energy Sustainability, Universiti Malaysia Sarawak, 94300 Kota Samarahan, Sarawak, Malaysia. Email: yibrahim@unimas.my.

Abstract

Technologies for the reduction of nitric oxide (NO) are well established and are a critical resource in reducing the emission of nitrogen oxides (NO_x) released during combustion. Herein, we demonstrate a more sustainable approach, utilising Earth-abundant metals supported on waste-derived carbon to facilitate this reaction. Selective catalytic reduction (SCR), whereby a reductant is used to convert NO over a catalytic bed into nitrogen, is regarded as the best available technology for NO reduction. Here, we have investigated the use of H_2, which has the potential to be produced from sustainable resources, as the reductant. Three selected *d*-metals (copper, iron and manganese) were impregnated over palm kernel shell activated carbons via incipient wetness. The characteristics of the carbon support and the derivative catalysts were analysed to investigate structure-performance relationships. H_2-SCR was performed in a fixed-bed reactor; the results showed that the supported-copper catalyst converted NO completely at temperatures of 250 °C and above. This is attributed to the high reducibility and acidity of the catalyst as demonstrated via temperature-programmed reduction, ammonia-temperature programmed desorption, Fourier-transform infra-red spectroscopy and nitric oxide adsorption-desorption experiments. It is concluded that the carbon-supported *d*-metal catalysts are viable for use in H_2-SCR, thereby promoting a more sustainable approach to mitigating NO_x emissions.

Keywords

Carbon catalyst; NO_x removal; Waste-to-materials; Heterogeneous catalysis; Characterisation

Graphical Abstract

Declarations

Funding: This work was supported by the Ministry of Higher Education Malaysia and University Malaysia Sarawak (Fundamental Research Grant Scheme F02/FRGS/2022/2020). The authors would like to acknowledge EPSRC award EP/K001329/1 for granting access to SEM-EDS. This research also used the resources of the Advanced Photon Source, a U.S. Department of Energy Office of Science User Facility operated for the DOE Office of Science by Argonne National Laboratory under Contract No. DE-AC02-06CH11357.

Financial interest: The authors have no relevant financial or non-financial interests to disclose.

Availability of data and material: The datasets generated during and/or analysed during the current study are available from the corresponding author on reasonable request.
Code availability: Not applicable.
Authors' contributions: IY: Conceptualisation, methodology, investigation, funding acquisition, writing (original draft). JMcG: Supervision, writing (reviewing and editing)
Ethics approval: Not applicable.
Consent to participate: Not applicable.
Consent for publication: Not applicable.

Novelty statement

Hydrogen selective catalytic reduction, as an alternative to the conventional ammonia selective catalytic reduction, is often used with resource-scarce precious metals. Herein, Earth-abundant *d*-metal catalysts supported over carbon derived from oil palm waste have been demonstrated. The novelty resides in the combination of waste valorization and application of Earth-abundant catalysts in a sustainable NO_x mitigation system.

1.0 INTRODUCTION

The mitigation of NO_x emissions is a well-established field in, e.g. the automotive sector. However, the emergence of waste-to-energy schemes necessitates the development of suitable and, crucially, sustainable technologies to reduce NO_x emissions. The generation of energy through the combustion or incineration of waste has the twin benefits of: (i) reducing societal reliance on fossil sources for heat and energy generation; and (ii) of providing an effective waste remediation strategy, thereby reducing the volume of material that is sent to landfill. Such schemes have hence increased in popularity; Figure 1 shows the growth in waste-to-energy market revenue over recent years for both thermal and biological technologies. A downside of utilizing waste in this way however is the generation of air pollutants such as nitrogen oxides (NO_x) during combustion. There is therefore the need to implement emission control technologies. These should be cost-effective and, crucially, sustainable in order to retain the environmental and ecological benefits of the waste-to-energy process. Selective catalytic reduction is one of the most effective available technologies currently used to degrade NO_x [1]. The most common methods of SCR utilise ammonia or urea as reducing agents [2], which bring safety and environmental issues such as ammonia slip, and require the use of noble metals such as Pt, Pd and Rh. These metals are both expensive and subject to significant resource constraints. There is therefore a necessity to develop novel catalyst systems based not on resource-scarce or unsustainable materials, but on Earth-abundant metals and waste or renewable feedstocks. This challenge is tackled in the present work.

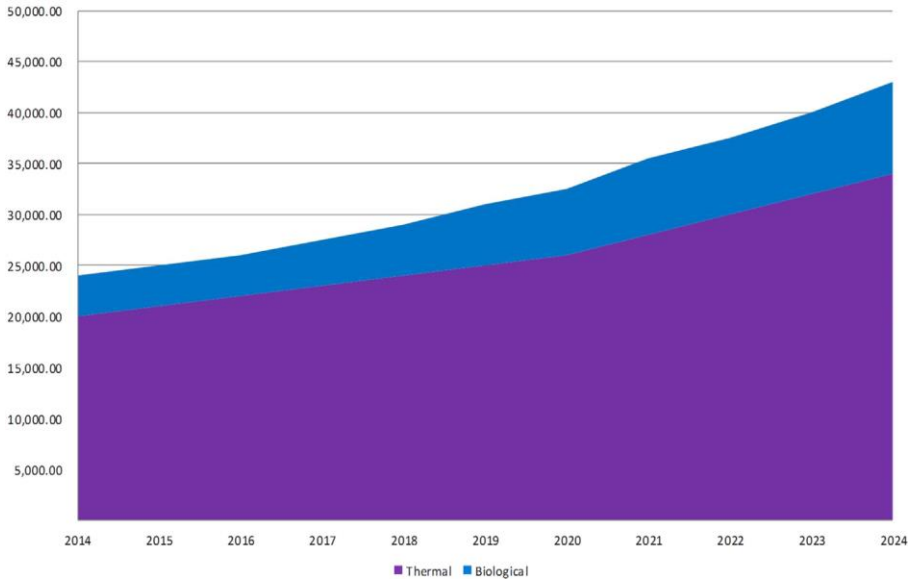

Figure 1. Global waste-to-energy market revenue [3] (reproduced with permission)

In addition to considering the nature of the catalyst, the sustainability of NO_x reduction can be further improved through considering alternative reductants to NH_3. An alternative reducing agent is hydrogen. The current environmental footprint of hydrogen production notwithstanding, it has the potential to be generated through sustainable routes in the future such as water electrolysis. The use of H_2 eliminates concerns around, e.g. ammonia slip which is deemed unacceptable in many countries [4]. Despite these advantages, research on H_2-SCR has largely concentrated on employing scarce and/or precious metals, in particular platinum group metals, as the active catalyst [5], [6]. A key reason for the efficacy of such catalysts is the strong interaction between NO molecules and the precious metals. *d*-Block metals however also present a strong interaction with NO and therefore have the potential to be effective catalysts in this reaction [7]. The efficacy of *d*-block metals in NO_x SCR can be ascribed to the electronic interaction between the reactant and the catalyst. As the NO $2\pi^*$ orbital consists of an unpaired electron and the transition metals have valence electrons in the *d*-subshell, metal-NO backbonding can take place from the metal *d*-orbital to the NO $2\pi^*$ orbital. This interaction is stronger than the N-O bond [8]. Furthermore, *d*-block metals such as iron, copper and manganese are well established to effectively activate H_2, being widely employed as hydrogenation catalysts [9]–[11]. Many alternative transition metals have been

investigated for NO_x SCR. Cr, Co and Ni however present health and environmental issues; e.g. Ni reacts with CO in the exhaust gas to form nickel tetracarbonyl, a product more toxic than CO [12]. Among other transition metals, Cu, Fe and Mn have shown promising and practical use as SCR catalysts with up to 100% conversion and selectivity [7], [13], [14]. These *d*-metals are also abundant in the Earth's crust as compared to platinum-group metals, providing ecological and economic advantages. For instance, copper is at least 4000 times cheaper than palladium, while iron is 2000 times cheaper than ruthenium [15].

The nature of the catalyst support also plays a crucial role; catalysts can exhibit enhanced performance due to the surface chemistry of the support and synergistic effects imposed by the support-metal bonding [16], [17]. Activated carbon has previously been investigated as a catalyst support in SCR [18]. Its high surface area and rich surface functional groups contribute to the reduction of NO [19], [20]. Activated carbon also has the advantage that it can be synthesized directly from waste biomass feedstocks such as palm kernel shell (PKS), coconut shell and rice husk. PKS is an abundant agricultural waste in palm oil producing countries and its utilization in those countries can help to address issues around waste accumulation and remediation [21]. Despite these advantages, the utilization of *d*-metals supported over activated carbon has not yet been extensively explored in H_2-SCR. This work seeks to address this through exploring the potential of Earth-abundant base metal catalysts supported on PKS-derived carbons for H_2-SCR. The objective is to provide a sustainable solution to emissions control from waste-to-energy processes and other related systems.

2.0 MATERIALS AND METHODS

2.1 Catalyst preparation

Palm kernel shell activated carbon (PKS) was obtained from a local supplier in Sarawak, Malaysia. The monometallic oxide catalysts were prepared via incipient wetness where the ratio of the carbon pore volume to the precursor metal salt solution is 1:1. As the pore volume of the PKS is ~0.5 ml/g (Table 1), 1 mL of deionized water was used for impregnation of every 2 g of PKS. The precursor metal salt solutions were

prepared using deionized water (18-20 µS/cm), copper nitrate trihydrate, iron nitrate nanohydrate and manganese dinitrate hydrate (Sigma-Aldrich, UK, 99.999% trace metals). The theoretical metal loading selected for synthesis was 10 wt.%. While a wide range of metal loadings have been studied in the literature, numerous studies have investigated a metal loading of 10 wt.% [22]–[24]. The selection of 10 wt.% in the present work therefore allows comparison with previous studies. Additionally the relatively low metal content is consistent with the aim of developing more sustainable catalysts through minimising resource utilisation. After impregnation, the catalysts were then calcined at 350, 510 and 540 °C, respectively, under static helium for two hours. The resulting catalysts were designated as PKS*M* where *M* = Cu, Fe and Mn.

2.2 Catalyst characterisation

The carbon support (i.e. PKS) and the derivative catalysts (PKSM) were characterised based on surface morphology, elemental composition, surface area and pore volume, catalyst acidity, crystalline phase, redox properties, and nitric-oxide adsorption-desorption.

Scanning electron microscopy with energy-dispersive X-ray spectroscopy (SEM-EDS) was used to characterise the surface morphology and elemental distribution on metal oxides-impregnated activated carbon. The calcined and reduced catalysts were studied employing a SEM-EDS JSM-6010LA (Jeol, USA) at 1000 magnification and 20 kV. Carbon, hydrogen, and nitrogen content was determined using a CHNS Flash elemental analyser 2000 (CE instrument, UK) and the oxygen content was obtained by the difference between the balance of the mass in this analysis and the ash content determined from a thermogravimetric analysis using TGA 4000 (PerkinElmer, UK). 5 mg of sample was placed in an aluminium capsule for combustion in the elemental analyser at 900 °C with 50 vol.% oxygen flow. A thermal conductivity detector equipped gas chromatograph (GC-TCD) was used to measure the resulting gases. For TGA, 5 mg of sample was heated to 950 °C in a controlled combustion chamber and held at this temperature until a plateau of mass loss was obtained. The metal loading on all synthesized catalysts was measured in comparison to the theoretical loading using an atomic absorption spectrometer AAS Analyst 400 (PerkinElmer, UK). The digestion of the

solid catalysts was performed according to the modified dry ash method, as previously described [25]. 5 mL of each sample was injected into the AAS.

The surface area and pore properties for the PKS and the catalysts were determined using nitrogen adsorption-desorption conducted on a 3Flex (Micromeritics, USA). Approximately 0.1 g of the samples were vacuum-dried in a VacPrep 061 sample degas system (Micromeritics, USA). Subsequently, a nitrogen adsorption-desorption experiment was carried out at 77 K. The surface area and pore volume were calculated using Brunauer-Emmett-Teller (BET) method, and t-plot and Barrett-Joyner-Halenda (BJH) methods, respectively. Wide-angle X-ray scattering (WAXS) was employed to determine the crystalline phase and size of the supported metal particles present in the synthesised catalysts. This was carried out at the Advanced Photon Source, a U.S. Department of Energy (DOE) Office of Science User Facility, at Argonne National Laboratory. Powdered samples were sandwiched in scotch tape prior to analysis. WAXS generates a diffraction pattern in 2D image that can be converted into a 1D data for analysis [26].

The catalyst acidity was analysed from the desorption profile of NH_3 (NH_3-TPD) at elevated temperature. 5 vol.% NH_3/He was pre-adsorbed on the catalyst surface as a basic probe at 20 mL/min prior to the experiment, conducted in a Chemisorb 2720 (Micromeritics, USA). After that, the samples were heated at 10 °C/min to 600 °C, where the evolved gases were detected at a thermal conductivity detector (TCD). In addition, the microtextural properties of the catalysts that influence their acid-base character have also been evaluated via attenuated total reflection (ATR) Fourier-transform infra-red spectroscopy (FTIR) conducted in an IRAffinity-1S FTIR spectrophotometer (Shimadzu, UK). The nature of the metal species (oxidation states) on the catalyst and the catalyst reducibility were determined using temperature-programmed reduction (H_2-TPR) analysis in the same equipment as NH_3-TPD, but with hydrogen as the gas probe. 60 mg of sample was heated with a temperature ramp of 10 °C/min in 20 mL/min of 5 vol.% H_2/Ar. Hydrogen was detected by the TCD giving a profile of hydrogen released as a function of temperature.

In addition, the nature of NO adsorption over the catalyst was also investigated to identify the types of adsorption species formed over the different metal species supported

on carbon. This was achieved via a NO-temperature-programmed desorption (NO-TPD) experiment. After exposure to 1 % NO/He until equilibrium, 0.2 g of sample was purged for at least 1 h to remove the physisorbed and trapped NO in the system. Upon desorption at increasing temperature, the evolved gases were detected by mass spectrometry (Hiden HPR-20, UK).

2.3 Catalyst activity testing

For determination of the conversion and selectivity, an isothermal reaction was performed on the catalysts at selected temperatures using a fixed-bed reactor as shown in Figure 2. The bed temperature is monitored using a type-K thermocouple inserted from the top of the reactor. All gases introduced into the reactor are controlled by mass flow controllers (MFC). Control and monitoring took place via a data acquisition system. 1 g of the pre-dried catalyst was loaded into the reactor, and purged using helium prior to any reaction. The catalyst was reduced *in-situ* at 250 °C under 5 % H_2/He at 250 sccm (equivalent to 7,175 h^{-1}). Then, the system was purged and cooled under pure helium flow to 40 °C. After increasing the temperature to the desired value, a gas mixture of 500 ppm NO + 4 % H_2 + 1.5 % O_2 in helium at 250 sccm was fed into the reactor and the reaction was allowed to reach steady-state at the reaction temperature for at least 2 h. The effluent was analysed continuously using a mass spectrometry MS (Hiden HPR-20, UK) and the quantification method used was based on a developed algorithm shown in Figure S.1.

The mole balance for nitrogen (as NO_x is the limiting reactant) can be written as per Equation 1, where F is the molar flow rate; F_p is the molar flow rate of the N-products including N_2, N_2O, NO_2 and NH_3; a is the number of nitrogen moles in the product molecule; P_{ads} is the number of moles of adsorbed NO_x or N-products which are not emitted from the reactor; and $NO_{x,gen}$ is the NO_x generated during the process. A positive mole difference between the measured inlet NO_x and the outlet NO_x, as well as the outlet N-products, is indicative of adsorption, while a negative value is indicative of NO_x generation. NO_x conversion (Equation 2) is calculated as the ratio of the total NO_x consumed to the amount of NO_x introduced into and generated within the system at steady-state conditions (at least after 60 minutes, as observed in this study). An efficient

SCR catalyst should be able to convert the adsorbed NO_x and release the N-products rapidly enough to avoid permanent occupancy of the active sites [5]. This is taken into consideration when calculating the efficiency of a new catalyst, termed here as selectivity towards N_2 formation, which is taken as the ratio of formed N_2 to the other products, including adsorbed species (Equation 3). In addition to NO conversion and N_2 selectivity, the combustion rate was also calculated based on the cumulative production of CO and CO_2.

$$F_{NO_x,in} = F_{NO_x,out} + \sum aF_p + \sum P_{ads} - NO_{x,gen} \quad (1)$$

$$Conversion, X\ (\%) = \frac{F_{NO_x,in} + NO_{x,gen} - F_{NO_x,out}}{F_{NO_x,in} + NO_{x,gen}} \times 100\% \quad (2)$$

$$Selectivity, S_{N_2}(\%) = \frac{2 \times F_{N_2}}{\sum aF_p + \sum P_{ads}} \times 100\% \quad (3)$$

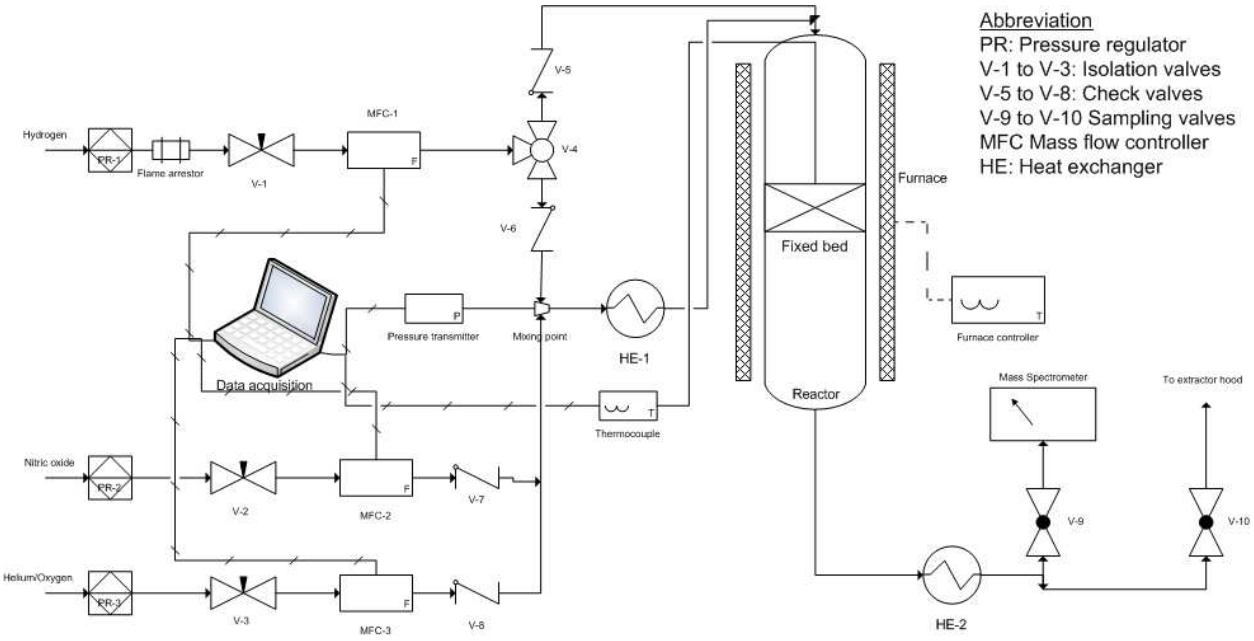

Figure 2. Experimental set-up for catalyst activity testing

3.0 RESULTS AND DISCUSSION

3.1 Catalyst characterisation

The measured surface properties of the catalyst support (PKS) and the catalysts are shown in Table 1. The surface area of PKS is >1000 m^2/g; values of this magnitude are common for activated carbons [27]. The total pore volume was ~0.5 cm^3/g with 80 % of the porosity being constituted by micropores. The nitrogen adsorption-desorption curve hysteresis loop (Figure S.2) indicated that the pores were mostly narrow slit-like [28] which can also be observed in the SEM micrograph (Figure 3a). The surface area of supported catalysts is lower than bare PKS. This suggest that the metal oxides are deposited on the surface such that they block larger pores. The observed 90% reduction in external surface area but relatively unchanged micropore volume supports this hypothesis. Notably, PKSFe has the smallest BET surface area, micropore area and volume and external surface area. Inspection of the SEM micrograph (Figure 3c) shows that this is due to micropores being blocked by large metallic deposits. In contrast, more micropores and interstices can be observed on PKSCu and PKSMn (Figure 3b and 1d, respectively).

Table 1. Surface properties for PKS and the derivative catalysts.

Properties (unit)	PKS	PKSCu	PKSFe	PKSMn
BET surface area (m^2/g)	1126	850	715	800
t-plot micropore area (m^2/g)	910	830	697	777
t-plot external surface area (m^2/g)	216	20	18	23
t-plot micropore volume (cm^3/g)	0.361	0.421	0.360	0.401
BJH adsorption average pore width (Å)	64	4	4	4

The elemental compositions of the catalysts are summarized in Table 2. PKS exhibits a high carbon content (82%), comparable with commercial activated carbons [29]. After metal impregnation the C:H ratio significantly increased suggesting that the presence of the metal catalyses the carbonisation of the PKS. Meanwhile, the ash content increased due to the presence of metals and incombustible matter after catalyst synthesis. The metal loadings were determined by AAS and are also shown in Table 2. In all cases they are close to the theoretical loading.

The acidic and redox properties of the catalysts are shown in Table 3. The acidity of PKS derives from its ash content and surface functional groups, as investigated by FTIR (Figure 4). The acidity of the catalyst was directly measured by NH_3-TPD (Figure 5). PKS exhibited large NH_3 desorption (i.e. the area under the peak normalised to the corresponding surface area) indicative of the intrinsic NH_3 adsorption sites due to the high acidity of the activated carbon. The acidity of activated carbon is known to be correlated with the presence of surface oxygenated functional groups [30], the presence of which has been confirmed herein by FTIR spectroscopy (Figure 4). Deconvolution of the NH_3-TPD peak revealed peaks for PKS at 220, 290, 370 and a shoulder between 400 and 500 °C (Figure S.3).

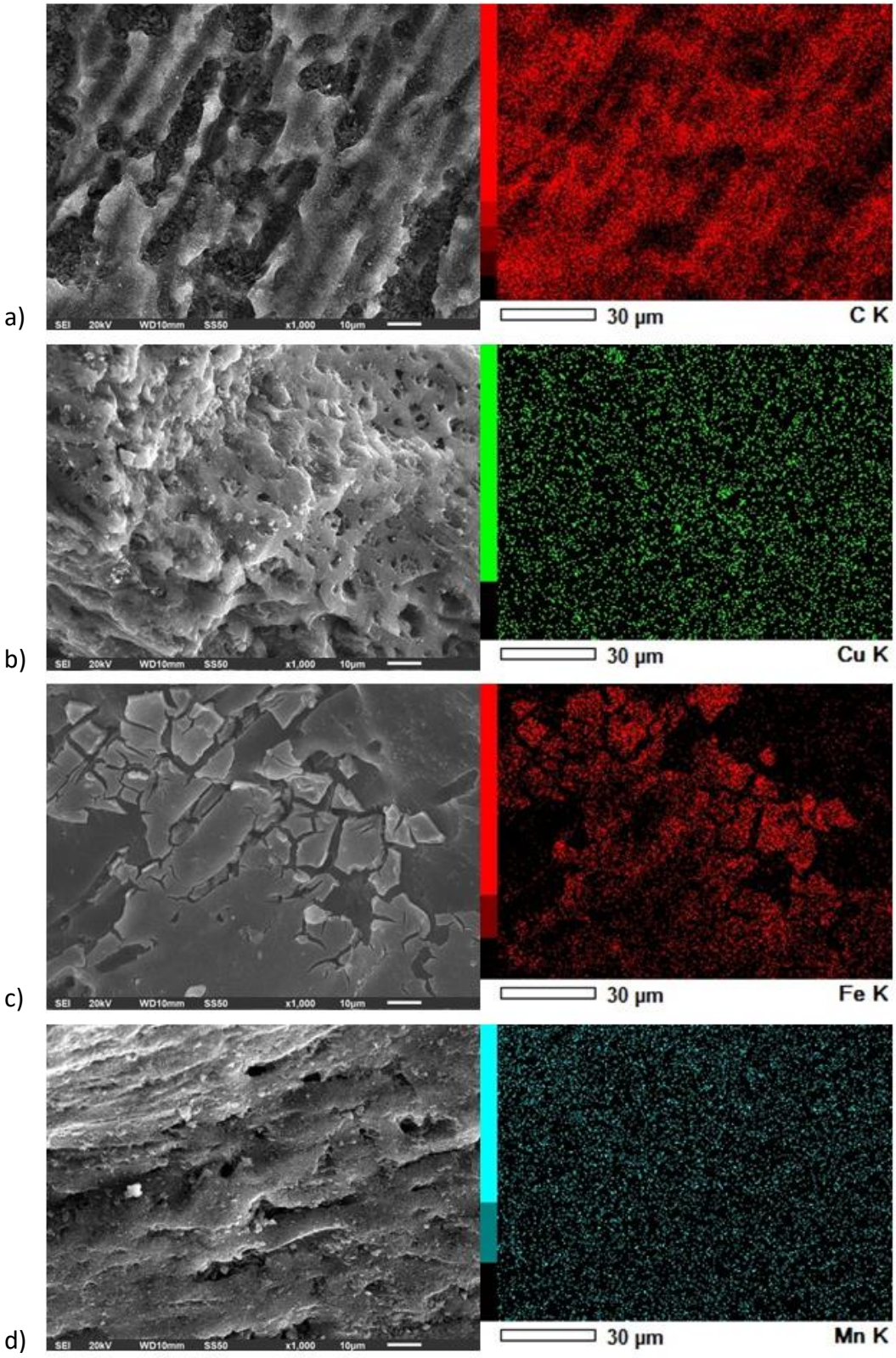

Figure 3. Scanning electron microscope micrographs and energy dispersive X-ray mapping (SEM-EDX) for a) PKS, b) PKSCu, c) PKSFe and d) PKSMn.

Table 2. Elemental composition for PKS and the derivative catalysts.

Element	Mass percentage (%) ± standard deviation (%)			
	PKS	**PKSCu**	**PKSFe**	**PKSMn**
C	82 ± 4	78 ± 2	75 ± 1	80 ± 1
H	1.15 ± 0.44	0.45 ± 0.01	0.52 ± 0.08	0.34 ± 0.02
N	0.89 ± 0.04	0.54 ± 0.03	0.49 ± 0.01	0.51 ± 0.05
O*	14.97	10.81	14.00	7.81
Ash	1.2 ± 0.8	10.6 ± 0.7	10.3 ± 1.3	11.3 ± 1.3
Doped metal percentage (%)**	-	8.3 ± 0.2	7.6 ± 1.2	6.1 ± 0.1

*From balance. **From atomic absorption spectroscopy.

Table 3. Chemical properties for PKS and the derivative catalysts.

Properties (unit)	PKS	PKSCu	PKSFe	PKSMn
Acidity				
Concentration of desorbed NH_3 ($X10^{-3}$ mmol/g)	7.12	9.59	2.01	5.44
Redox properties				
Total H_2 consumption ($X10^{-3}$ mmol/g)	0	2.75	0.53	0.34
Reducibility ($X10^{-3}$/°C)	-	5	2.9	4.5
Offset temperature (°C)	500	350	370	335

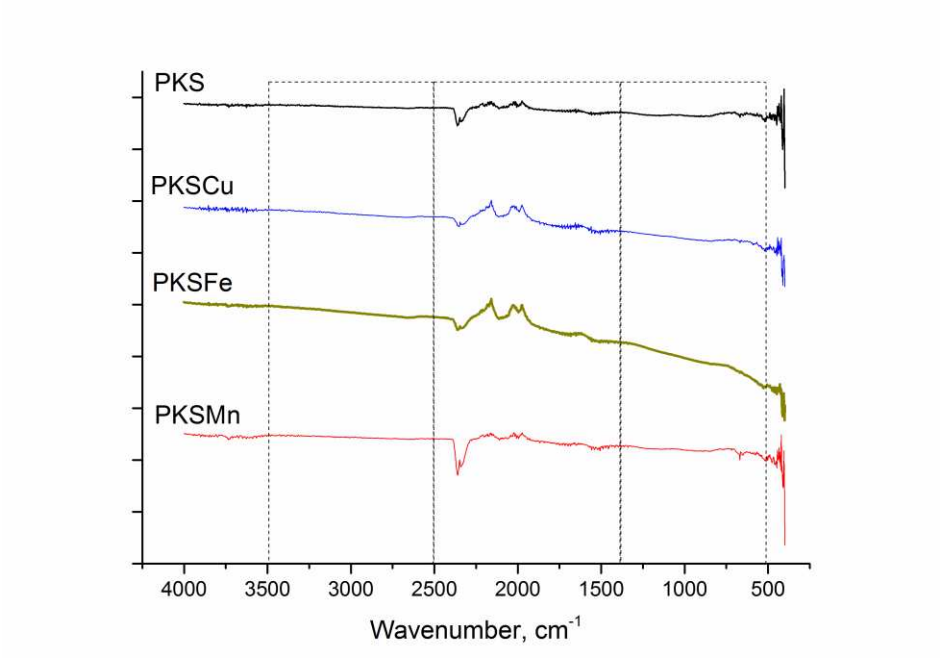

a)

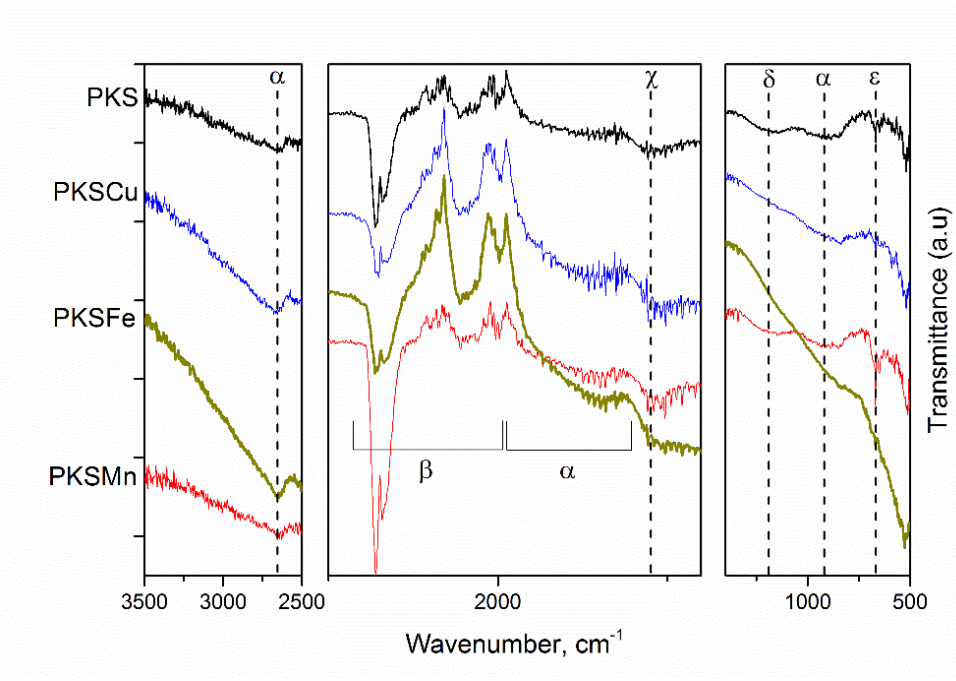

b)

Figure 4. a) Full FTIR spectra (4 cm^{-1} resolution at 16 scans), and b) Magnified FTIR regions for PKS and the derivative catalysts. α: carboxylic acids, β: alkyne, χ: aromatics, δ: aliphatic amines and ε: alkene.

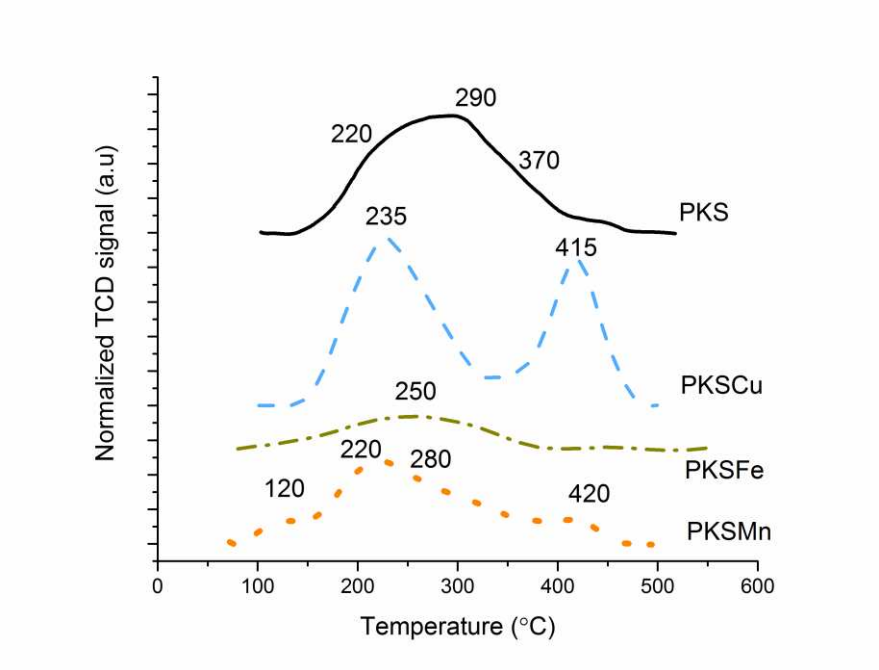

Figure 5. NH_3-TPD profiles for PKS and the derivative catalysts in 20 sccm pure helium and 10 °C/min.

Impregnation of PKS with the metal oxides reduced the acidity of the carbon support, suggesting that the metal oxides bind to the surface at acidic moieties. Additionally, calcination may also result in the loss of some sites [27]. Multiple desorption peaks are observed for all materials; notably PKSCu, exhibits two distinct peaks centred around 235 and 415 °C. A previous study on the acidity of copper supported over SAPO-34 showed that the desorption peaks shifted to lower temperature upon loading the metal [31]. Specifically, two peaks at ~150 and ~450 °C observed over the bare support shifted to 140 and 320 °C respectively after copper loading. The shift in the position of the NH_3-desorption peaks for PKSCu relative to PKS in the present work can similarly be ascribed to the presence of copper. It is also known from the literature that the sharp peak at around 200 °C can be assigned to weakly adsorbed NH_3 while the one at > 400 °C can be ascribed to strongly adsorbed NH_3 [32]. The area under the curve showed that PKSCu has higher acidity as compared to the PKS.

In contrast, the acidity of PKS was reduced after impregnation with iron and manganese due to the high calcination temperature used. This is in agreement with previous observations from Lee et al. who observed that manganese TPD peaks

decreased upon increasing the calcination temperature from 300 to 700 °C [33]. On the NH_3-TPD curve for PKSFe, only a wide and low desorption peak can be seen, extending from 100 to 400 °C (centred at 250 °C) alongside a shoulder from 400 to 500 °C, which is in a similar range to the peak observed for raw PKS. Fe/ZSM-5 has previously been reported to exhibit a NH_3-desoprtion peak at ~300 °C [34], [35]. This suggests that Fe may have only partially contributed to the adsorption of NH_3 alongside the carbon surface functional groups in the present study. The loss of functional groups from the carbon surface in the presence of Fe contributes to its low acidity, a conclusion supported by both FTIR spectroscopy (Figure 4) and SEM results (Figure 3).

The addition of manganese to PKS resulted in the appearance of four NH_3 desorption peaks (see Figure S.6 for deconvolution) at 120, 220, 280 and 420 °C. The first peak is ascribed to physisorbed NH_3, which is very weakly attached to the catalyst surface and can be disregarded as an acidic site [33]. Deng et al. examined a MnO_x/TiO_2 catalyst in a NH_3-TPD experiment and found two peaks associated with MnO_x acidic sites at 220 and 360 °C indicating the weak and strong acidic sites [13]. This suggests that the second (220 °C) and third (280 °C) peaks in the NH_3-TPD curve for PKSMn could be assigned to both PKS and Mn acidic functionalities while the fourth one (420 °C) is due to strongly acidic MnO_x sites.

FTIR spectroscopy was employed in order to characterise the surface functional groups present, which determine the acid/base properties of the catalysts. Full FTIR spectra for PKS and the carbon catalysts are shown in Figure 4a, while Figure 4b magnifies three regions (3500 to 2500 cm^{-1}, 2500 to 1400 cm^{-1} and 1400 to 500 cm^{-1}) to facilitate inspection. The presence of carboxylic acid functionalities (α) is indicated by the O-H stretch at ~2660 cm^{-1}, broad C=O stretches from 1970-1620 cm^{-1} and the 900 cm^{-1} O-H bend [36]. Carboxylic acids are Brønsted-Lowry acids due to their tendency to donate protons (H^+). Chen et al. also reported the presence of these moieties over a cerium-copper catalyst supported on ordered mesoporous carbon, while Gao et al. observed this group over a commercial activated carbon studied via X-ray photoelectron spectroscopy [30], [37], [38]. The other functional groups generally presence on the catalysts include alkyne groups (β) (2380-2000 cm^{-1}), aromatics (χ) (~1550 cm^{-1}), N-containing functional groups such as aliphatic amines (δ) (1200 cm^{-1}) and alkene moieties (ε) (670 cm^{-1}) [36].

Hong et al. reported that N-containing functional groups found over NH_3-functionalized activated carbon contributed to the adsorption of NO [39]. Consistent with SEM and NH_3-TPD studies it is notable that PKSFe shows carboxylic acid (α) content; confirming that the loading of Fe and subsequent calcination results in a loss of these groups and therefore reduces the acidity of the synthesised catalysts.

The reducibility of the catalyst was determined via TPR. Figure 6a shows the TPR profiles for the carbon-supported metal oxides and bare PKS for reference; Figure 6b shows deconvolution of the PKSCu profile. The presence of metal oxides increases hydrogen consumption, a key requirement for H_2-SCR reaction. The reduction temperature for the catalysts increases in the series PKSCu < PKSMn < PKSFe. The initial reduction of Cu^{2+} to Cu^{+} occurs at ~200 °C with a subsequent reduction at 230 °C assigned to the direct reduction of CuO to Cu (~63 % of the total integrated area) and a third peak at >330 °C corresponding to the reduction of Cu^{+} to Cu^{0}. Previous studies on copper supported on activated carbon prepared from coconut shell have reported a reduction temperature range of 150-300 °C with stepwise CuO reduction ($Cu^{2+} \rightarrow Cu^{+} \rightarrow Cu^{0}$) [40]. PKSMn exhibits two reduction peaks at 220 and 410 °C. According to Deng et al., the reduction of pure manganese oxide can be observed at two temperatures: 350 °C for MnO_2 to Mn_2O_3, and 520 °C for the successive Mn_2O_3 to MnO reduction [13]. Therefore, upon impregnation over PKS, both reduction temperatures are shifted to lower values. Notably, the greater hydrogen consumption for the second peak indicates that some Mn_2O_3 was already present on the catalyst surface due to the calcination process. For PKSFe a single reduction peak at 340 °C is observed, attributed to the reduction of Fe_2O_3 to Fe_3O_4. This is consistent with previous work by Patel et al. where Fe/MCM-41 exhibited peaks at 390 and 590 °C for the reduction of Fe_2O_3 to Fe_3O_4 and Fe_3O_4 to FeO, respectively [7]. Therefore, the temperatures applied in this work are insufficient to effect reduction to FeO.

WAXS studies have been conducted in order to gain insights into the crystal phase(s) of the deposited metal oxides on the catalyst surface. The WAXS patterns for PKS and the mono-metal oxide catalysts are shown in Figure 7. The baseline in the PKS diffractogram shown in the figure was not removed in order to highlight the amorphous phase of the activated carbon synthesized from biomass. Upon impregnation and

calcination of copper over PKS, crystallite growth of Cu, CuO, and Cu_2O was evident with crystalline planar Cu_2O [111] being the most dominant. Similar observations were reported by Kikhtyanin et al. [41], who reported the prevalent formation of Cu_2O species under inert calcination. In the case of iron and manganese, the crystal growths of the metal oxides were not as distinctive, with only Fe_2O_3 observed on PKSFe and Mn_2O_3 and MnO_2 on PKSMn. This contrasts with the findings of Everbroeck et al. [42] where Fe and Mn-based catalysts were synthesized via a co-precipitation method in a mixed metal oxides matrix.

At this point, it is interesting to correlate between the findings from H_2-TPR and WAXS. Both TPR and WAXS analysis of PKSCu showed the presence of CuO and Cu_2O, with WAXS additionally showing growth of Cu. This highlights the ability of WAXS to identify unreduced, crystalline, metal species on the catalyst. Note however that the intensity of a WAXS peaks should not be directly correlated with the amount of a given species; instead this is indicative of the tendency for the crystal to grow in a particular geometry [43]. In the case for PKSFe and PKSMn, both TPR and WAXS analysis indicated the presence of the same species on the PKS surface. TPR is however seen to be more sensitive for less crystalline phases.

The behaviour of the catalysts under oxidizing conditions was investigated by DTG (Figure 8). The loss of mass witnessed for all materials implies that gasification of the carbon occurred at elevated temperature. The inflection point for PKS occurs in excess of 600 °C, which is typical for bulk carbon gasification, temperature in air [44][45]. In the presence of the transition metals, the inflection point is lowered to ~400, ~410 and ~450 °C for PKSMn, PKSCu and PKSFe respectively. This demonstrates the ability of the metal oxides present to catalyse gasification with manganese exhibiting the greatest catalytic impact and iron the least. Elsewhere, the reverse trend was observed with Fe_2O_3 increasing the carbon ignition point by 27 % and MnO_2 by only 11 % [46]. However, in that work the metal oxides were mixed physically by mortar at 1.5 wt.%, which is different from the current study where the metal oxides were impregnated over the carbon surface via incipient wetness. The utilization of the catalysts beyond their offset temperature should be performed with caution due to the likely loss of carbon.

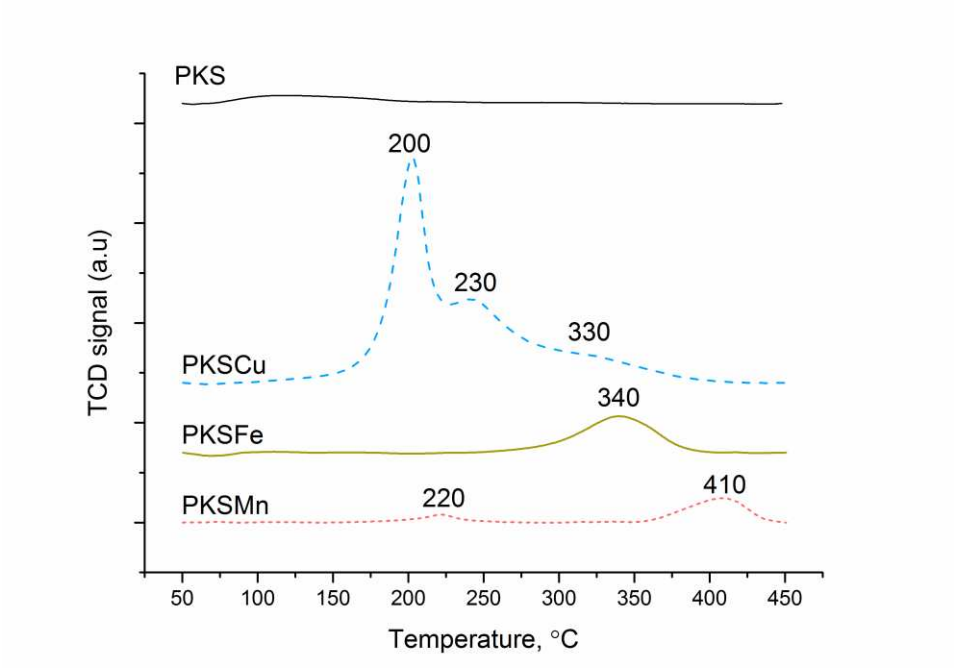

a)

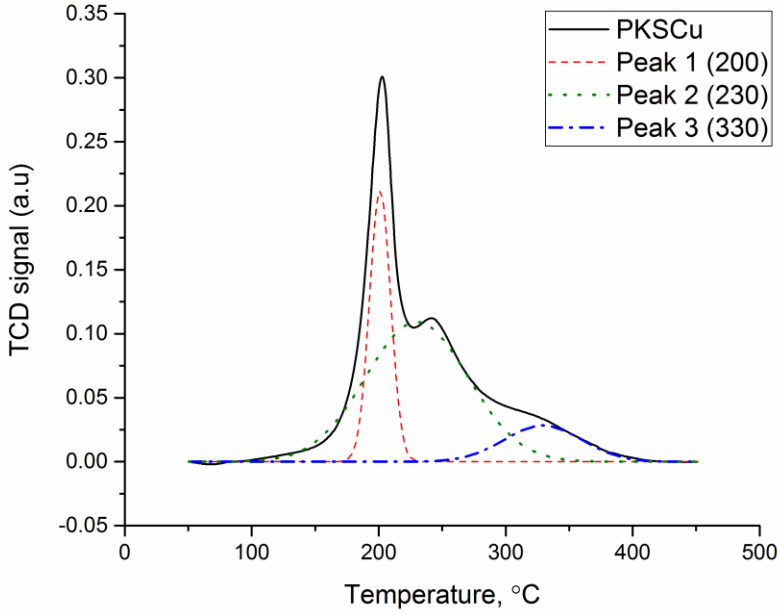

b)

Figure 6. a) H_2-TPR profiles for the PKS and carbon catalysts in 5 % H_2/He at 20 sccm and 10 °C/min, and b) H_2-TPR peak deconvolution for PKSCu using OriginPro 2017 with Gaussian peak model and Levenberg Marquardt iteration algorithm.

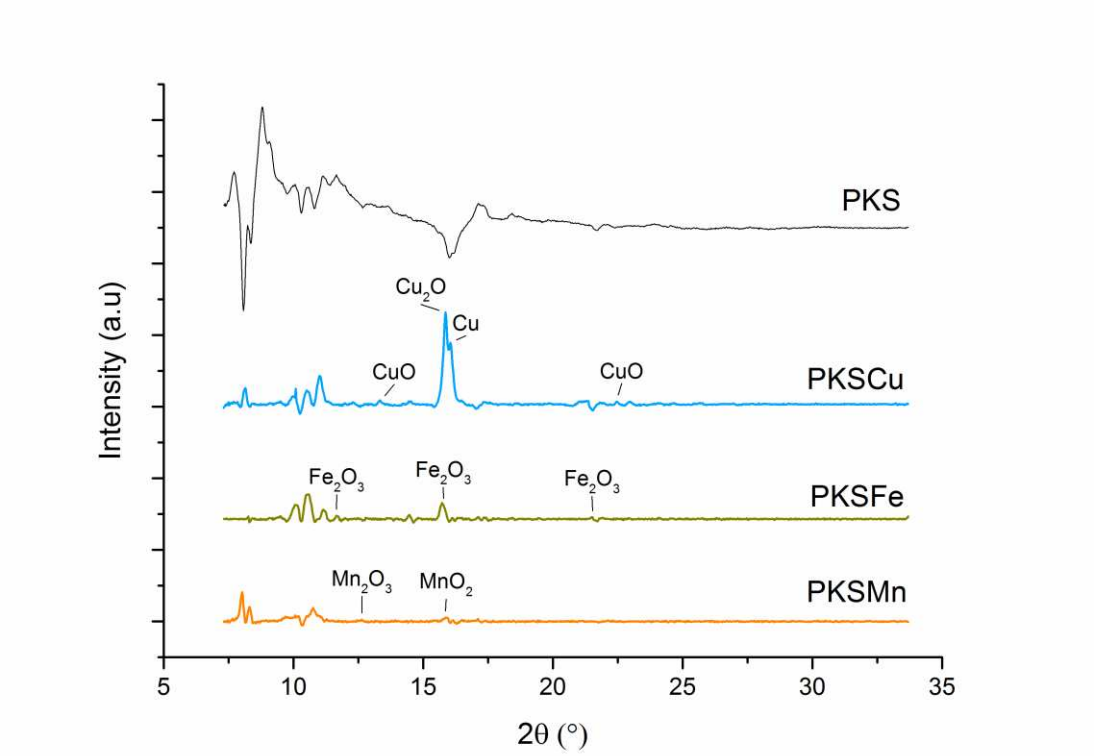

Figure 7. WAXS diffractograms for PKS and the derivative catalysts

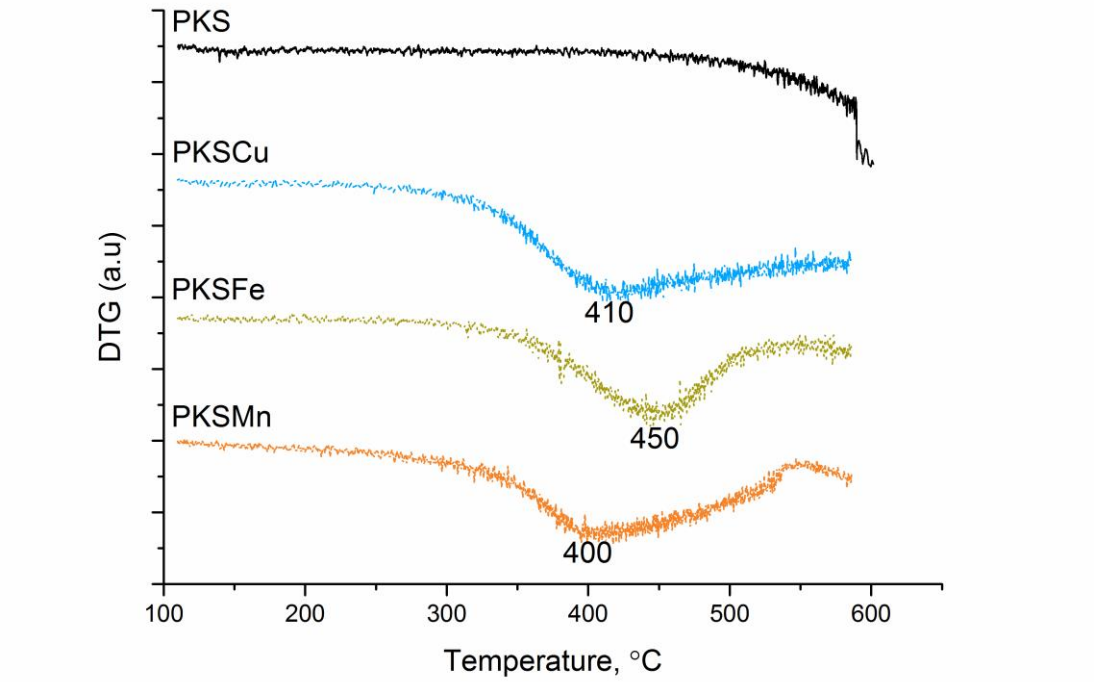

Figure 8. DTG curves for PKS and the derivative catalysts in 20 sccm air and 10 °C/min.

The characterisation of *d*-metals supported over PKS revealed that the catalyst synthesis reduced BET surface area and acidity of the carbon support, while increasing C:H ratio and ash content. The corroboration between FTIR and NH_3-TPD analysis indicates the presence of surface oxygenated functional groups and their contribution to the catalyst acidity. The metal species increased the hydrogen consumption by providing reducible sites for hydrogen. As a consequence, the offset temperatures for the catalysts were lowered with respect to the PKS.

3.2 Nitric oxide adsorption-desorption experiment

NO-TPD experiments were performed both on the bare carbon support and the *d*-metal supported catalysts. For PKS, nitric oxide and nitrogen dioxide were both observed to evolve from the surface upon heating (Figure 9). No other species such as nitrogen or nitrous oxide were detected. These data indicate that NO is readily adsorbed by PKS at room temperature, most likely at basic sites such as nitrogen functionalities on the carbon support [47]. This suggests that PKS has suitable chemical characteristics to act as a catalyst support in nitric oxide reduction. The lack of N_2O or N_2 evolution suggests that this adsorption is non-dissociative, in agreement with previous studies over using pyrolyzed sub-bituminous coal where NO desorbed with a wide TPD-peak centred at 300 °C and a shoulder at 400 °C [48]. Two NO desorption peaks are observed in the present work; a sharp peak at 165 °C and a broader peak at 270 °C. The former can be ascribed to the desorption of adsorbed NO_2, formed via oxidation over activated carbon which desorbs reductively [49]. The higher temperature peak can be assigned to strongly bonded NO. The evolution of small quantities of NO_2 at ~130 °C is a result of the decomposition of – $C(ONO_2)$ surface complexes [50] and indicates a degree of oxidation ability for bare PKS. Notably, CO_2 and CO also evolved during NO-TPD for PKS (curves not shown). As carbon is not readily oxidized in the absence of oxygen at low temperatures, it is proposed that this is due to surface complex decomposition (Equations 4 - 6), as previously proposed [50].

$$-C(ONO_2) \rightarrow CO_2 + NO \qquad 4$$

$$-C(ONO_2) \rightarrow C(O) + NO_2 \qquad 5$$

$$-C(ONO_2) \rightarrow CO + NO_2 \quad (6)$$

Figure 10 shows NO-TPD results from the carbon supported *d*-metal catalysts. In all cases, the quantity of adsorbed NO reduced at least 3-fold compared to the area under the peak of NO-TPD of PKS. No other N-products are observed during desorption. Incorporation of *d*-metals onto activated carbon therefore reduced the capacity for NO adsorption. The primary reason for this is the loss of carbon and nitrogen content, which provided adsorption sites for NO. The bond between NO and *d*-metals is not as strong as NO with the carbon support. This can be demonstrated by evaluating the desorption temperature peaks of each catalyst.

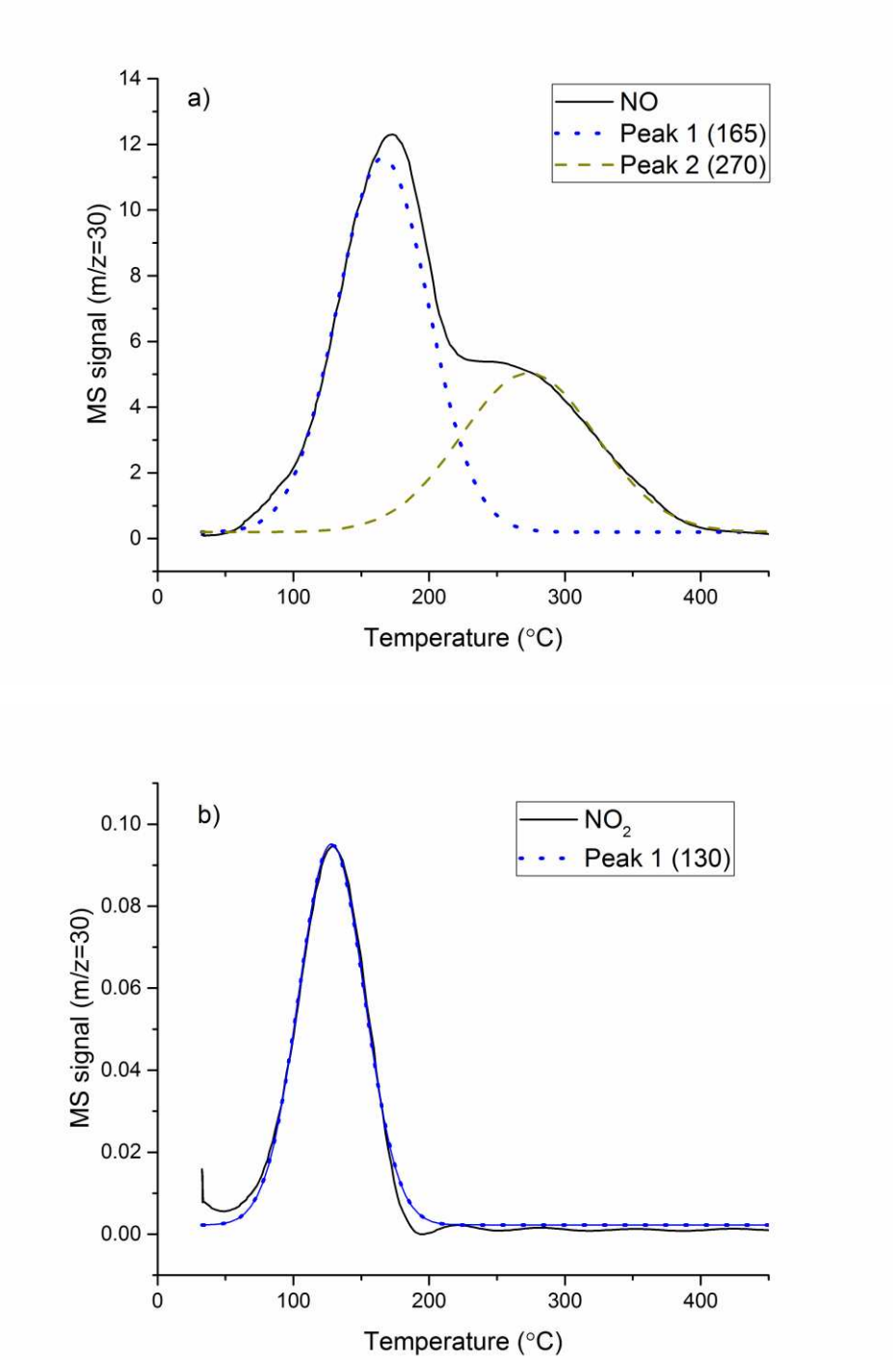

Figure 9. NO-TPD peak deconvolution for PKS showing evolved; a) NO and b) NO_2 in 20 sccm pure helium and 10 °C/min.

For PKSCu, NO desorption peaks were observed at ~85, ~115 and ~160 °C (Figure 10a). Wang et al. reported a desorption peak around 100 °C over Cu/CeO_2

catalysts ascribed to the presence of nitrosyl species bonded to copper [14]. Therefore, the first two peaks can be assigned to NO adsorbed on copper sites. The third peak, which has similar desorption temperature with Peak 1 in Figure 9a, can be assigned to adsorbed NO_2.

Considering PKSFe and PKSMn, both possessed an additional low-temperature peak at 90 and 70 °C, respectively. This is attributed to NO_x physisorbed on metal oxide sites as previously reported by Long & Yang and Lee et al. for Fe/ZSM-5 and Mn/TiO_2 respectively [33], [34]. The peak assigned to $–C(ONO_2)$ on PKS (130 °C) is shifted to lower temperature for PKSMn (115 °C), and to slightly higher temperature for PKSFe (134 °C). There is a high-temperature peak observed for PKSMn at 210 °C (Figure 10c), which can be postulated to be either the shifted adsorbed NO peak (Figure 9a), or the strong NO_x-Mn bond as reported by Kijlstra et al. which was observed at ~207 °C when studying NO-TPD over a MnO_x/Al_2O_3 catalyst [51]. Lower desorption temperature is correlated with lower adsorption energies, therefore C-N surface complexes possessed lower adsorption energy over metal-impregnated catalysts as compared to over the bare carbon support.

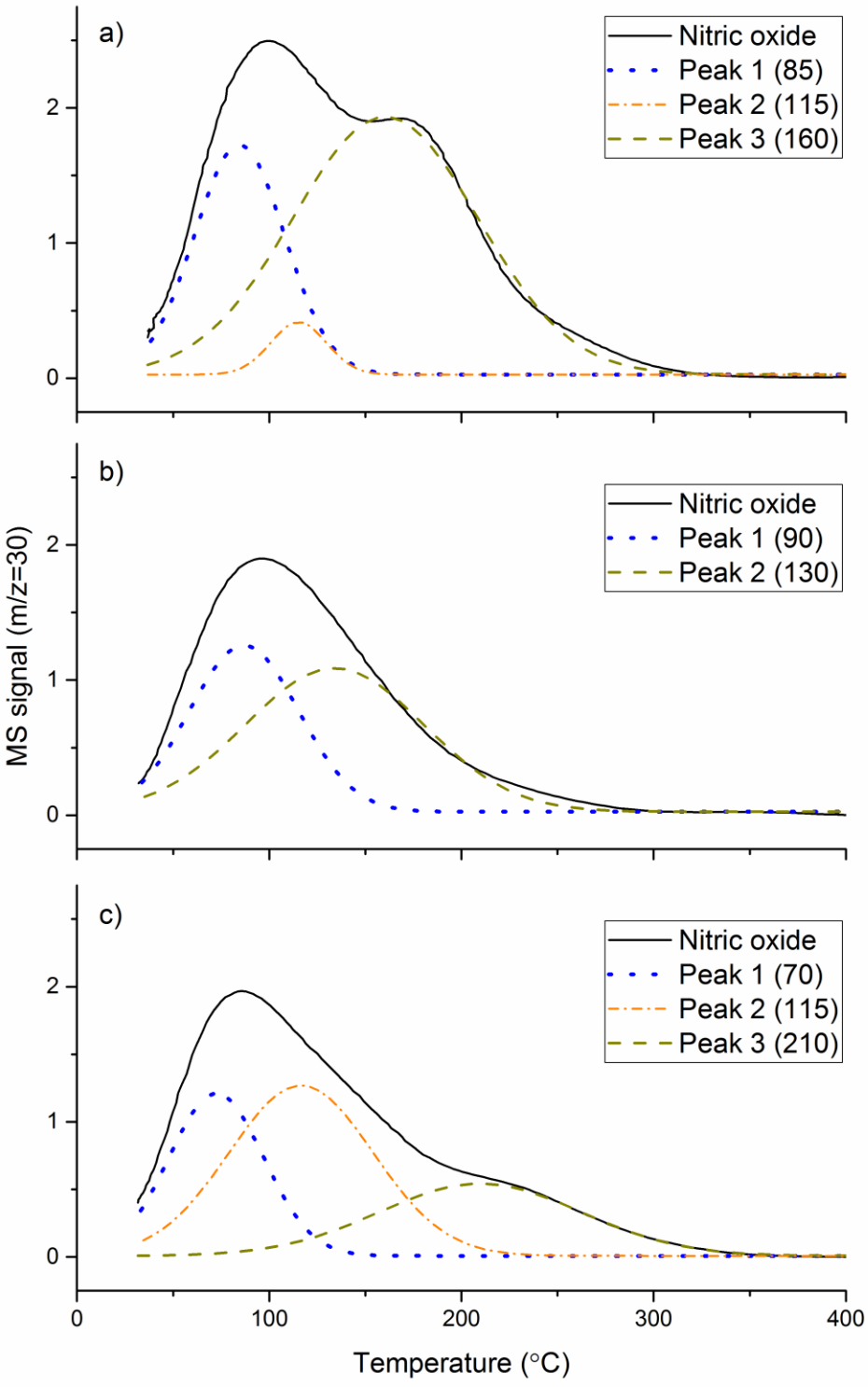

Figure 10. NO-TPD peak deconvolution for; a) PKSCu, b) PKSFe and c) PKSMn in 20 sccm pure helium and 10 °C/min.

Additionally, there was no NO_2 evolved during NO-TPD over any of the three catalysts. This suggests that the desorption of the formed NO_2 was reductive due to the presence of reductive sites (S_{red}), according to Equations 7 and 8 [49].

$$(NO_2)_{ads} + S_{red} \rightarrow NO + CO \quad (7)$$

$$2(NO_2)_{ads} + S_{red} \rightarrow NO + CO_2 \quad (8)$$

The area under the peak indicates the quantity of NO adsorption species at a particular site. By taking the amount of nitrosyls formed per gram of metal, it can be inferred that the formation of this species is most pronounced over PKSCu, followed by PKSFe and PKSMn. This is not correlated to the order of decreasing acidity even accounting for the fact that NO is reported to adsorb at Brønsted acid sites. Therefore, the formation of nitrosyls over carbon-supported catalysts can be considered somewhat complex; its contributions as a reaction intermediate are not the focus of this work. It is however conclusive that NO was readily adsorbed over PKS. The bond was stronger than the nitrosyl species formed over *d*-metal catalysts. The weak nitrosyl bond would allow further dissociation with a reductant in gaseous phase, and avoid permanent occupation of the adsorption sites thus resulting in facile regeneration of these sites.

3.3 Gasification of catalysts in NO-H_2-O_2 system

An important feature of a carbon-supported catalyst is the rate of carbon combustion due to oxidation by the intrinsic oxygen present in the flue gas and/or oxides of nitrogen. Figure 8 showed that the offset temperature of the carbon catalysts reduced considerably with the impregnation of metals. In the present work, the rate of gasification of carbon was calculated based on the accumulative rate of CO_2 and CO formation in μmol/s during H_2-SCR; the results are shown in Figure 11. Generally, the combustion rate for all catalysts increased with increasing temperature, from an average of 0.2 μmol/s at 250 °C to an average of 0.55 μmol/s at 300 °C.

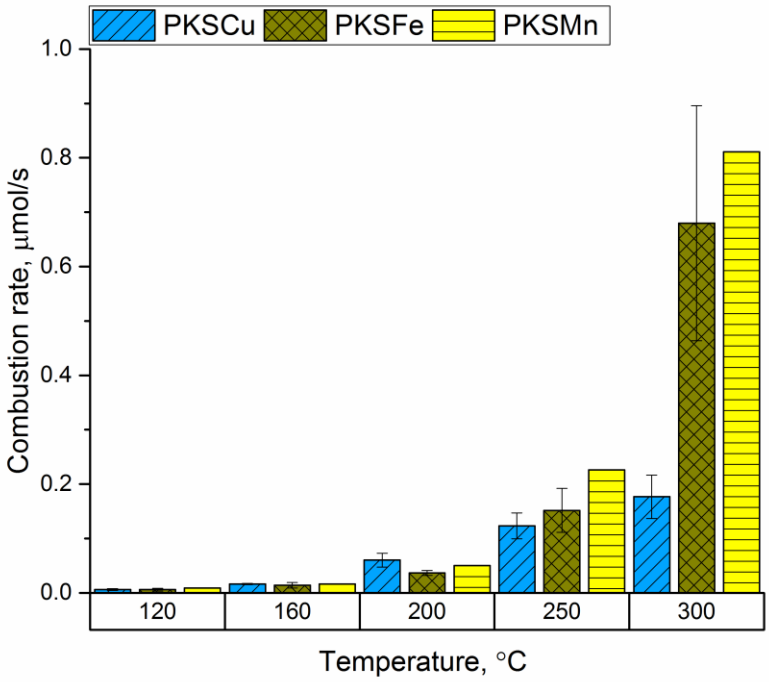

Figure 11. Combustion rate by the catalysts in 500 ppm NO + 4 % H_2 + 1.5 % O_2 at 7,175 h^{-1}.

The order of decreasing combustion rate at 300 °C (close to the offset temperature) is PKSMn ≈ PKSFe > PKSCu[1]. This may be a consequence of the fact that the electropositivity of the reduced metal states (the catalysts were reduced in hydrogen flow prior to this experiment) also decreases in this order [52]. High electropositivity indicates a higher tendency for the metal to donate electrons which increases the electron density of neighbouring carbon sites (C). This leads to the increased affinity of this site for binding an oxygen atom, C_f. As a result, C-C_f bonds are weakened and carbon gasification is promoted. The information provided by the combustion rate can be a determining factor for catalyst application in a particular oxidizing environment. The loss of carbon through gassification can influence the reusability of the catalyst as the carbon provides surface area, anchoring sites for the catalyst, acidic surface functional groups and adsorption sites for the reaction, as discussed in Sections 3.1 – 3.3. Based on the

[1] Note the standard deviation for PKSFe is only significant at high temperature 300 °C. This might be due to another factor, such as catalyst dispersion, contributing to the combustion rate. This was not investigated further due to the absence of this effect in other samples.

calculated gasification rates, PKSCu, PKSFe and PKSMn could lose 50% of their initial carbon mass (approximately 0.45 g) in 104, 30 and 26 h, respectively. Shen, Ge and Chen reported a carbon xerogel catalyzing NO_x reduction was stable up to 166 h [53].

3.4 Catalyst activity

Prior to evaluation of the supported catalysts, the activity of the bare PKS was tested. Figure 12 shows the evolution of NO in the temperature range 50 – 200 °C. Product formation is negligible at all temperatures. At lower temperatures (below 150 °C) there was a decrease in NO signal, indicating adsorption. Isothermal experiments were conducted at 120, 160, 200, 250 and 300 °C.

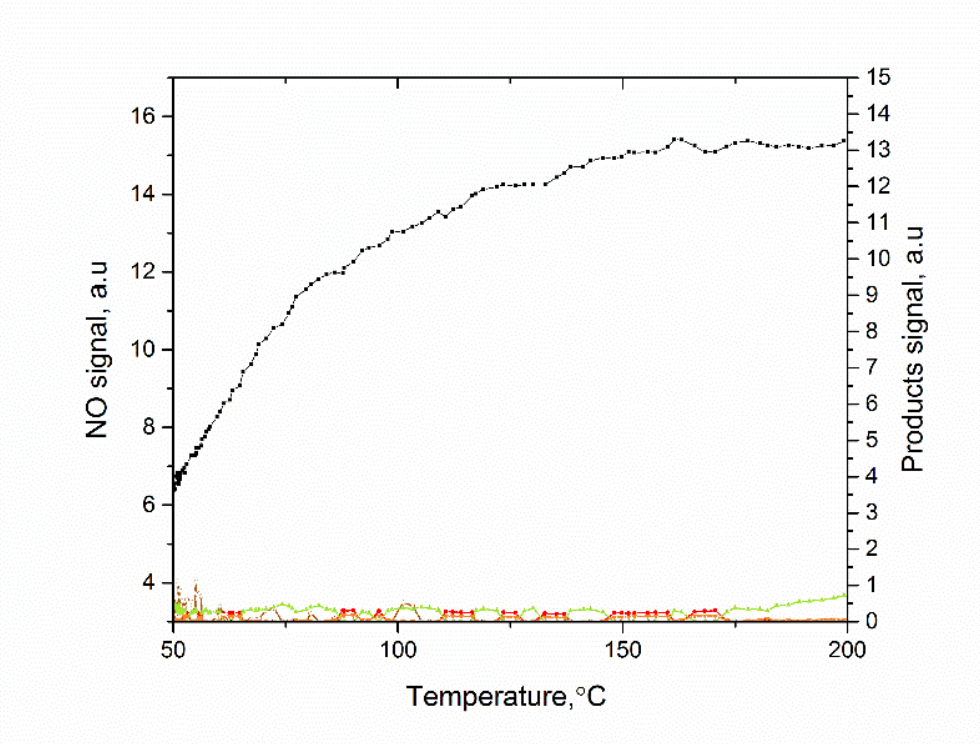

Figure 12. Temperature-programmed reactions for PKS at 7,175 h^{-1} and 1 °C/min in; 500 ppm NO + 4 % H_2 + 1.5 % O_2. (■) Nitric oxide, (●) nitrous oxide, (♦) nitrogen, (◊) ammonia, (○) nitrogen dioxide, (▲) carbon dioxide, and (▼) carbon monoxide.

Figure 13 shows NO conversion over the three catalysts in the presence of NO, H_2 and O_2. All catalysts are seen to achieve higher conversion at elevated temperatures, but only PKSCu showed 100% conversion of NO below 300 °C. PKSFe and PKSMn exhibited low conversion activity at low temperatures until 250 °C, above which the

conversion exceeded 20 % for PKSFe and 10 % for PKSMn. These findings indicate that the *d*-metals supported over activated carbon are able to facilitate the reduction of NO using hydrogen as an alternative reducing agent but at varying levels of efficiency.

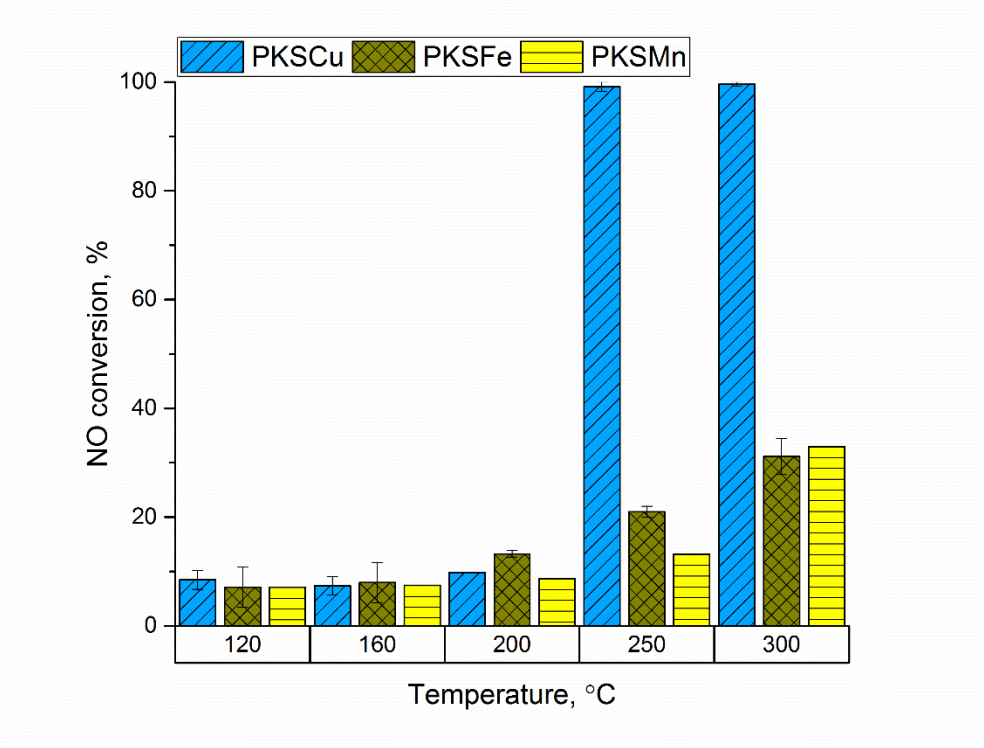

Figure 13. Nitric oxide conversion by the catalysts in 500 ppm NO + 4 % H_2 + 1.5 % O_2 at 7,175 h^{-1}.

It is clear from Figure 13 that at 250 and 300 °C, PKSCu gave the highest NO conversion (~100%) followed by PKSFe and PKSMn, but at 300 °C the activity of the catalysts decreased in the order PKSCu > PKSMn ≈ PKSFe. Noble metal catalyst such as platinum, supported on carbon, have previously shown similar performance but at much lower temperature (160 °C) [4]. Table 4 shows the performance of Cu, Fe and Mn-based catalysts from selected studies using ammonia, urea or carbon monoxide as a reductant which can be compared to the use of H_2 in the present work. In NH_3-SCR, Cu, Fe and Mn supported over activated carbon have previously been shown capable of achieving 100% reduction of NO_x at 200, 420, and 250 °C, respectively [54]–[56].

The order of catalyst activity at high temperature is consistent with the findings on the reducibility of the catalyst (Section 3.1). It is known that catalyst reducibility is an

important factor in NO_x reduction. As oxygen mobility is increased on a reducible metal surface, oxygen vacancies are easily generated [57], [58]. This is required for the dissociation of adsorbed NO over metal surfaces. The removal of oxygen from this vacancy will keep the metal reduced for the next reaction cycle [59].

Table 4. Comparison between selected literature studies and this present study using Cu, Fe and Mn-based catalysts.

Catalyst	Feed gas composition	Highest NOx conversion (%) / temperature (°C)	Reference
10%Cu/PKS	500ppm NO + 4% H_2 + 1.5% O_2 + N_2	100 / 250	Present study
10%Fe/PKS	500ppm NO + 4% H_2 + 1.5% O_2 + N_2	28 / 300	Present study
10%Mn/PKS	500ppm NO + 4% H_2 + 1.5% O_2 + N_2	33 / 300	Present study
$Cu/CePO_4$	700ppm NO + 700ppm NH_3 + 5% O_2 + N_2	100 / 250	[60]
21%Cu/activated carbon	540ppm NO + 680ppm NH_3 + 2% O_2 + He	100 / 200	[54]
10%Fe/active carbon	800 ppm NO + 800 ppm NH_3 + 3% O_2 + He	100 / 420	[55]
3%Mn/rice straw char	1000 ppm NO + 1000 ppm NH_3 + 5% O_2 + N_2	100 / 250	[56]
Mn-Ce-Fe/coal-based activated coke	0.04% NO + 0.04% NH_3 + 7.2% O_2 + N_2	84 / 220	[19]
12%Mn/nutshell activated carbon	550ppm NO + 6% CH_4N_2O + 16% O_2 + N_2	90 / 50	[61]
$10\%Fe/TiO_2$	400ppm NO + 400ppm CO + 2% O_2 + He	30 / 200	[22]
$5\%Cu/AlPO_4$	0.2% NO + 0.65% O_2 + 1.5% CO + He	100 / 325	[62]
$3\%Fe\text{-}Mo/Al_2O_3$	1000ppm NO + 1% O_2 + 4% CO + He	80 / 700	[63]

In addition, the observed trend in reactivity may also correlate with the acidity of the catalysts as shown by NH_3-TPD analysis and the quantity of nitrosyl formation as shown by NO-TPD. NH formation during the reaction of NO/H_2 over metallic surfaces is well-known. PKSCu, which showed the highest amount of adsorbed ammonia among the three catalysts in NH_3-TPD studies, provides more sites for the intermediates to be adsorbed and consumed. PKSCu also exhibited the highest nitrosyl formation (NO adsorbed over metal oxides) which also contributed to the high conversion.

Figure 14 shows the variation of N_2 selectivity over the catalysts. The decrease in selectivity was due to the release of ammonia in the outlet where ammonia is known to be an important intermediate in H_2-SCR. The formation of NO_2 and N_2O is negligible across the entire experiment (not shown). As can be seen from the graph, PKSCu showed

the highest formation of NH_3, followed by PKSFe. The selectivity towards N_2 formation over PKSCu peaked at ~100 % at 200 °C, reducing by 40% at 250 °C. At 300 °C, selectivity for PKSCu increased to ~100 %. PKSFe followed a similar trend, except that beyond 250 °C the selectivity remained constant.

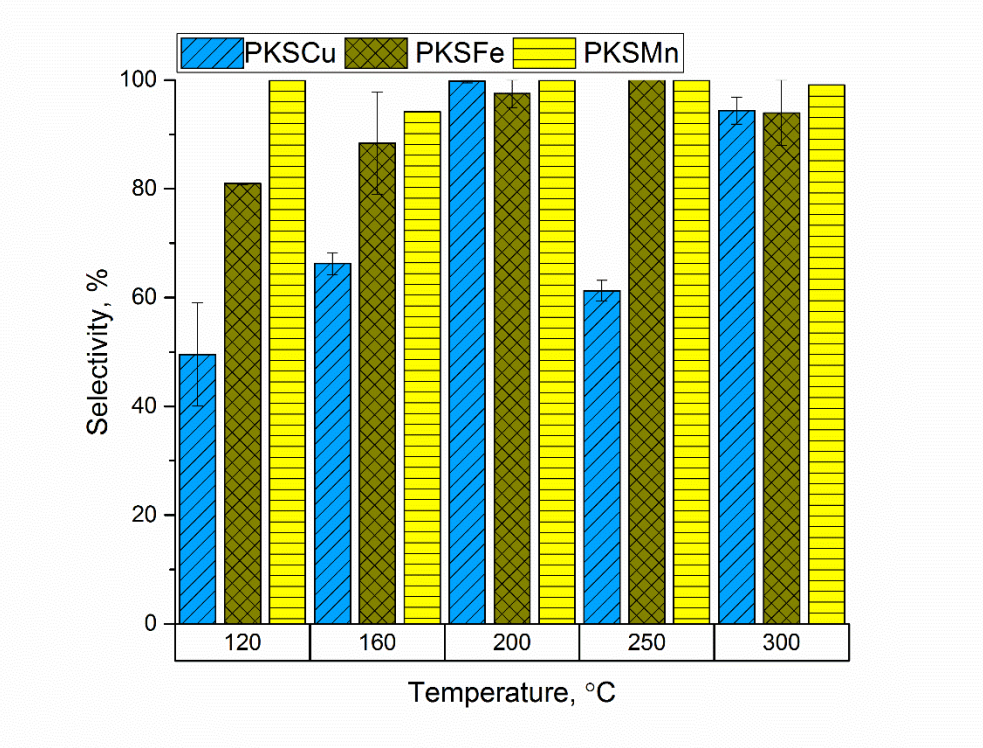

Figure 14. Nitrogen selectivity by the catalysts in 500 ppm NO + 4 % H_2 + 1.5 % O_2 at 7,175 h^{-1}.

The high selectivity achieved by PKSFe and PKSMn throughout the temperature range does not imply high reactivity in H_2-SCR compared to the other catalysts as lower conversion is achieved. It is postulated that over iron and manganese, insufficient NH intermediate is produced. N_2-selectivity values must solely be used to make sure the catalysts do not produce additional toxic gases in addition to NO_x. Therefore, despite the relatively lower cost of Fe relative to Cu, Cu is preferred as a catalyst in this system. A potential interesting subject for future investigation is the design and evaluation of mixed-metal catalysts to optimise both conversion and selectivity. The selection of a catalysts in terms of the selectivity must be made with caution.

On another note, the formation of by-products when using PKSCu as the catalyst must be investigated further in terms of the mechanism. Based on the characterisation and reaction studies presented herein, the proposed mechanism for NO_x reduction is as follows: NO is adsorbed over acidic sites (provided by both carbon support and copper oxides) as nitrosyl, and then dissociates to N and O over the sites due to the stronger metal *d*-orbital to NO $2\pi^*$ orbital backbonding (as compared to N-O bond). The introduction of H_2 as the reductant forms NH as intermediate, which can further form NH_3 via equations 9 – 12. This ammonia further reacts with NO (adsorbed and unadsorbed) to finally form N_2 and H_2O via equation 13.

$$M - NO + M - H \rightarrow M - NH + M - O \quad (9)$$

$$M - NH + H_2 \rightarrow M + NH_3 \quad (10)$$

$$M - NO + M - H \rightarrow M - N + M - OH \quad (11)$$

$$M - N + {}^{3}/_{2}\, H_2 \rightarrow M + NH_3 \quad (12)$$

$$4NO + 4NH_3 + O_2 \rightarrow 4N_2 + 6H_2O \quad (13)$$

4.0 CONCLUSIONS

Carbon-supported *d*-metal catalysts were synthesized using palm kernel shell activated carbon as the support, and copper, iron and manganese as the active metals. NO was found to adsorb over the carbon support as adsorbed NO_2 and strongly adsorbed NO species. Upon impregnating the carbon with metal oxides, the extent of NO adsorption reduced as did the extent of NO oxidation, while the formation of nitrosyl species over the metal surfaces was evident. The impregnation and calcination in the synthesis stage produced Cu, Cu_2O and CuO species over PKSCu, MnO_2 and Mn_2O_3 species over PKSMn and Fe_2O_3 species over PKSFe as determined from TPR. PKSCu was the most facile to reduce followed by PKSMn and PKSFe; this trend correlates with an increase in NO conversion. The catalyst acidity and the quantity of nitrosyls formed were also seen to affect the activity in H_2-SCR. High catalyst acidity (as found in PKSCu) provided more sites for NH (an intermediate in H_2-SCR) adsorption and reaction with the formed nitrosyls over the catalyst surface. In addition, PKSMn showed the highest carbon

combustion activity due to high electropositivity compared to the other two *d*-metals. This information is valuable in developing a structure-performance relationship of a H_2-SCR catalyst.

Acknowledgement

This work was supported by the Ministry of Higher Education Malaysia and University Malaysia Sarawak under the Fundamental Research Grant Scheme F02/FRGS/2022/2020]. The authors would like to acknowledge EPSRC award EP/K001329/1 for granting access to SEM-EDS. This research also used the resources of the Advanced Photon Source, a U.S. Department of Energy Office of Science User Facility operated for the DOE Office of Science by Argonne National Laboratory under Contract No. DE-AC02-06CH11357. Special thanks goes to Prof. Greg Beaucage and his students (Alex McGlasson, Michael Chauby, and Kabir Rishi) at the University of Cincinnati for their assistance in WAXS analysis, and Dr Jan Ilavsky and his team, who run and operate the beamline at Argonne.

References

[1] B. Johnke, “Emissions From Waste Incineration,” *Good Pract. Guid. Uncertain. Manag. Natl. Greenh. Gas Invent.*, pp. 455–468, 1996.

[2] M. Piumetti, S. Bensaid, D. Fino, and N. Russo, “Catalysis in diesel engine NO_x aftertreatment: a review,” *Catal. Struct. React.*, vol. 1, no. 4, pp. 155–173, 2015.

[3] L. Makarichi, W. Jutidamrongphan, and K. anan Techato, “The evolution of waste-to-energy incineration: A review,” *Renew. Sustain. Energy Rev.*, vol. 91, no. November 2017, pp. 812–821, 2018.

[4] B. Tu, N. Shi, W. Sun, L. Cao, and J. Yang, “SO_2-tolerant and H_2O-promoting Pt/C catalysts for efficient NO removal via fixed-bed H_2-SCR,” *Environ. Sci. Pollut. Res.*, vol. 24, no. 1, pp. 676–684, 2017.

[5] Z. Liu, F. Yu, C. Ma, J. Dan, J. Luo, and B. Dai, “A critical review of recent progress and perspective in practical denitration application,” *Catalysts*, vol. 9, no. 9, 2019.

[6] V. K. Patel and S. Sharma, “Effect of oxide supports on palladium based catalysts

for NO reduction by H_2-SCR," *Catal. Today*, Article In Press, 2020.

[7] A. Patel, P. Shukla, T. E. Rufford, V. Rudolph, and Z. Zhu, "Selective catalytic reduction of NO with CO using different metal-oxides incorporated in MCM-41," *Chem. Eng. J.*, vol. 255, pp. 437–444, 2014.

[8] S. Roy, M. S. Hegde, and G. Madras, "Catalysis for NO_x abatement," *Appl. Energy*, vol. 86, no. 11, pp. 2283–2297, 2009.

[9] S. Weber, J. Brünig, L. F. Veiros, and K. Kirchner, "Manganese-Catalyzed Hydrogenation of Ketones under Mild and Base-free Conditions," *Organometallics*, vol. 40, no. 9, pp. 1388–1394, 2021.

[10] B. Sahoo *et al.*, "A robust iron catalyst for the selective hydrogenation of substituted (iso)quinolones," *Chem. Sci.*, vol. 9, no. 42, pp. 8134–8141, 2018.

[11] N. Azri, R. Irmawati, U. I. Nda-Umar, M. I. Saiman, and Y. H. Taufiq-Yap, "Effect of different supports for copper as catalysts on glycerol hydrogenolysis to 1,2-propanediol," *J. King Saud Univ. - Sci.*, vol. 33, no. 4, p. 101417, 2021.

[12] J. R. Mondt, *Cleaner cars: The History and Technology of Emission Control Since the 1960s*. Warrendale: Society of Automotive Engineers, 2000.

[13] S. Deng *et al.*, "Advanced MnO_x/TiO_2 Catalyst with preferentially exposed anatase (001) facet for low-temperature SCR of NO," *ACS Catal.*, vol. 6, pp. 5807–5815, 2016.

[14] X. Wang, W. Wen, Y. Su, and R. Wang, "Influence of transition metals (M = Co, Fe and Mn) on ordered mesoporous CuM/CeO_2 catalysts and applications in selective catalytic reduction of NO_x with H_2," *RSC Adv.*, vol. 5, no. 77, pp. 63135–63141, 2015.

[15] NRCCSR, "Replacing critical materials with abundant materials - the role of the chemical sciences in finding alternatives to critical resources," 2012.

[16] E. Japke, M. Casapu, V. Trouillet, O. Deutschmann, and J. D. Grunwaldt, "Soot and hydrocarbon oxidation over vanadia-based SCR catalysts," *Catal. Today*, vol. 258, pp. 461–469, 2015.

[17] B. Guan, R. Zhan, H. Lin, and Z. Huang, "Review of state of the art technologies of selective catalytic reduction of NO_x from diesel engine exhaust," *Appl. Therm. Eng.*, vol. 66, no. 1–2, pp. 395–414, 2014.

[18] B. Shen, J. Chen, S. Yue, and G. Li, “A comparative study of modified cotton biochar and activated carbon based catalysts in low temperature SCR,” *Fuel*, vol. 156, pp. 47–53, 2015.

[19] Y. Li *et al.*, “Denitrification performance of non-pitch coal-based activated coke by the introduction of MnO_x–CeO_x–M (FeO_x, CoO_x) at low temperature,” *Mol. Catal.*, vol. 445, pp. 21–28, 2018.

[20] S. Bai, S. Jiang, H. Li, and Y. Guan, “Carbon nanotubes loaded with vanadium oxide for reduction NO with NH_3 at low temperature,” *Chinese J. Chem. Eng.*, vol. 23, no. 3, pp. 516–519, 2015.

[21] N. Hamzah, K. Tokimatsu, and K. Yoshikawa, “Solid fuel from oil palm biomass residues and municipal solid waste by hydrothermal treatment for electrical power generation in Malaysia: A review,” *Sustain.*, vol. 11, no. 4, pp. 1–23, 2019.

[22] T. Boningari, S. M. Pavani, P. R. Ettireddy, S. S. C. Chuang, and P. G. Smirniotis, “Mechanistic investigations on NO reduction with CO over Mn/TiO_2 catalyst at low temperatures,” *Mol. Catal.*, vol. 451, pp. 33–42, 2018.

[23] S. Binti, I. Anthonysamy, S. B. Afandi, M. Khavarian, A. Rahman, and B. Mohamed, “A review of carbon-based and non-carbon-based catalyst supports for the selective catalytic reduction of nitric oxide,” *J. Nanotechnol.*, no. 2, pp. 740–761, 2018.

[24] J. Lou, C. Hung, and L. Huang, “Selective Catalytic Reduction of NO by Methane on Copper Catalysts : the Effects of Modifying the Catalysts with Acids on γ - alumina,” *Aerosolo Air Qual. Res.*, vol. 3, no. 1, pp. 61–73, 2003.

[25] A. Enders and J. Lehmann, “Comparison of wet-digestion and dry-ashing methods for total elemental analysis of biochar,” *Commun. Soil Sci. Plant Anal.*, vol. 43, no. 7, pp. 1042–1052, 2012.

[26] Ilavsky, J., Zhang, F., “Development of combined microstructure and structure characterization facility for in situ and operando studies at the Advanced Photon Source,” *J. Appl. Crystallogr.*, vol. 51, pp. 867–882, 2018.

[27] M. A. Yahya *et al.*, “A brief review on activated carbon derived from agriculture by-product,” in *AIP Conference Proceedings*, 2018, vol. 1972, pp. 1–8.

[28] K. S. W. Sing *et al.*, “Reporting physisorption data for gas/solid systems with

special reference to the determination of surface area and porosity (Recommendations 1984)," *Pure Appl. Chem.*, vol. 57, no. 4, pp. 603–619, 1985.

[29] A. S. S. Al-Rahbi, M. A. Nahil, C. Wu, and P. T. Williams, "Waste-derived activated carbons for control of nitrogen oxides," *Proc. Inst. Civ. Eng. - Waste Resour. Manag.*, vol. 169, no. 1, pp. 30–41, 2016.

[30] J. Chen, F. Cao, R. Qu, X. Gao, and K. Cen, "Bimetallic cerium-copper nanoparticles embedded in ordered mesoporous carbons as effective catalysts for the selective catalytic reduction of NO with NH_3," *J. Colloid Interface Sci.*, vol. 456, pp. 66–75, 2015.

[31] T. Yu, D. Fan, T. Hao, J. Wang, M. Shen, and W. Li, "The effect of various templates on the NH_3-SCR activities over Cu/SAPO-34 catalysts," *Chem. Eng. J.*, vol. 243, pp. 159–168, 2014.

[32] S. Han, J. Cheng, Q. Ye, S. Cheng, T. Kang, and H. Dai, "Microporous and Mesoporous Materials Ce doping to Cu-SAPO-18 : Enhanced catalytic performance for the NH_3 -SCR of NO in simulated diesel exhaust," *Microporous Mesoporous Mater.*, vol. 276, no. May 2018, pp. 133–146, 2019.

[33] S. M. Lee, K. H. Park, S. S. Kim, D. W. Kwon, and S. C. Hong, "Effect of the Mn oxidation state and lattice oxygen in Mn-based TiO_2 catalysts on the low-temperature selective catalytic reduction of NO by NH_3," *J. Air Waste Manage. Assoc.*, vol. 62, pp. 1085–1092, 2012.

[34] R. Q. Long and R. T. Yang, "Temperature-programmed desorption/surface reaction (TPD/TPSR) study of Fe-exchanged ZSM-5 for selective catalytic reduction of nitric oxide by ammonia," *J. Catal.*, vol. 198, pp. 20–28, 2001.

[35] A. Lindholm, H. Sjövall, and L. Olsson, "Reduction of NO_x over a combined NSR and SCR system," *Appl. Catal. B Environ.*, vol. 98, no. 3–4, pp. 112–121, 2010.

[36] J. L. White, "Interpretation of infrared spectra of soil minerals," *Soil Sci.*, vol. 112, no. 1, pp. 22–31, 1971.

[37] L. Yuan *et al.*, "The effect of preparation conditions of Pt/Al_2O_3 on its catalytic performance for the H_2-SCR in the presence of oxygen," *Front. Environ. Sci. Eng.*, vol. 7, no. 3, pp. 457–463, 2013.

[38] X. Gao, S. Liu, Y. Zhang, Z. Luo, M. Ni, and K. Cen, "Adsorption and reduction of

NO_2 over activated carbon at low temperature," *Fuel Process. Technol.*, vol. 92, no. 1, pp. 139–146, 2011.

[39] Z. Hong, Z. Wang, and X. Li, "Catalytic oxidation of nitric oxide (NO) over different catalysts: An overview," *Catal. Sci. Technol.*, vol. 7, no. 16, pp. 3440–3452, 2017.

[40] J. C. Moreno-Piraján, J. Tirano, B. Salamanca, and L. Giraldo, "Activated carbon modified with copper for adsorption of propanethiol," *Int. J. Mol. Sci.*, vol. 11, no. 3, pp. 927–942, 2010.

[41] O. Kikhtyanin, V. Pospelova, J. Aubrecht, M. Lhotka, and D. Kubička, "Effect of atmosphere calcination and temperature on the hydrogenolysis activity and selectivity of copper-zinc catalysts," *Catalysts*, vol. 8, no. 10, 2018.

[42] T. Van Everbroeck, R. G. Ciocarlan, W. Van Hoey, M. Mertens, and P. Cool, "Copper-containing mixed metal oxides (Al, Fe, Mn) for application in three-way catalysis," *Catalysts*, vol. 10, no. 11, pp. 1–20, 2020.

[43] B. Fultz and J. Howe, *Transmission Electron Microscopy and Diffractometry of Materials*, Second Edi. Berlin: Springer-Verlag Berlin Heidelberg, 2002.

[44] D. Dollimore, T. A. Evans, Y. F. Lee, G. P. Pee, and F. W. Wilburn, "The significance of the onset and final temperatures in the kinetic analysis of TG curves," *Thermochim. Acta*, vol. 196, pp. 255–265, 1992.

[45] D. B. Radic, M. M. Stanojevic, M. O. Obradovic, and A. M. Jovovi, "Thermal analysis of physical and chemical changes occuring during regeneration of activated carbon," *Therm. Sci.*, vol. 21, no. 2, pp. 1067–1081, 2017.

[46] Yingjie Hu, Zhiqiang Wang, Xingxing Cheng, Ming Liu, and Chunyuan Ma, "Effects of catalysts on combustion characteristics and kinetics of coal-char blends," in *Asia Conference on Energy and Environment Engineering (ACEEE 18)*, 2018, pp. 1–7.

[47] R. Arrigo *et al.*, "Tuning the acid/base properties of nanocarbons by functionalization via amination," *J. Am. Chem. Soc.*, vol. 132, no. 28, pp. 9616–9630, 2010.

[48] D. López, R. Buitrago, A. Sepúlveda-Escribano, F. Rodríguez-Reinoso, and F. Mondragon, "Low-temperature catalytic adsorption of NO on activated carbon materials," *Langmuir*, vol. 23, pp. 12131–12137, 2007.

[49] W. Klose and S. Rincón, “Adsorption and reaction of NO on activated carbon in the presence of oxygen and water vapour,” *Fuel*, vol. 86, no. 1–2, pp. 203–209, 2007.

[50] M. Jeguirim, V. Tschamber, J. F. Brilhac, and P. Ehrburger, “Interaction mechanism of NO_2 with carbon black: effect of surface oxygen complexes,” *J. Anal. Appl. Pyrolysis*, vol. 72, pp. 171–181, 2004.

[51] W. S. Kijlstra, D. S. Brands, E. K. Poels, and A. Bliek, “Mechanism of the selective catalytic reduction of NO by NH_3 over MnOx/Al2O3. I. Adsorption and desorption of the single reaction components,” *J. Catal.*, vol. 171, pp. 208–218, 1997.

[52] L. Castoldi, R. Matarrese, L. Lietti, and P. Forzatti, “Intrinsic reactivity of alkaline and alkaline-earth metal oxide catalysts for oxidation of soot,” *Appl. Catal. B Environ.*, vol. 90, pp. 278–285, 2009.

[53] Y. Shen, X. Ge, and M. Chen, “Catalytic oxidation of nitric oxide (NO) with carbonaceous materials,” *RSC Adv.*, vol. 6, pp. 8469–8482, 2016.

[54] L. Singoredjo, M. Slagt, J. van Wees, F. Kapteijn, and J. A. Moulijn, “Selective catalytic reduction of NO with NH_3 over carbon supported copper catalysts,” *Catal. Today*, vol. 7, pp. 157–165, 1990.

[55] J. Pasel *et al.*, “Transition metal oxides supported on active carbons as low temperature catalysts for the selective catalytic reduction (SCR) of NO with NH_3,” *Appl. Catal. B Environ.*, vol. 18, no. 3–4, pp. 199–213, 1998.

[56] J. S. Cha *et al.*, “The low-temperature SCR of NO over rice straw and sewage sludge derived char,” *Chem. Eng. J.*, vol. 156, no. 2, pp. 321–327, 2010.

[57] Y. Cheng *et al.*, “Simultaneous NO_x and particulate matter removal from diesel exhaust by gierarchical Fe-doped Ce-Zr Oxide,” *ACS Catal.*, vol. 7, pp. 3883–3892, 2017.

[58] Y. Ji *et al.*, “Pt- and Pd-promoted CeO2-ZrO_2 for passive NO_x adsorber applications,” *Ind. Eng. Chem. Res.*, vol. 56, pp. 111–125, 2017.

[59] L. Ilieva *et al.*, “NO reduction by CO over gold catalysts supported on Fe-loaded ceria,” *Appl. Catal. B Environ.*, vol. 174–175, pp. 176–184, 2015.

[60] C. Liu *et al.*, “A comparative study of MO_x (M = Mn, Co and Cu) modifications over $CePO_4$ catalysts for selective catalytic reduction of NO with NH_3,” *J. Hazard.*

Mater., vol. 363, no. March 2018, pp. 439–446, 2019.

[61] K. Liu, Q. Yu, B. Wang, H. Xie, W. Duan, and Q. Qin, “Activated carbon-supported catalyst loading of CH_4N_2O for selective reduction of NO from flue gas at low temperatures,” *Int. J. Hydrogen Energy*, vol. 44, no. 26, pp. 13523–13537, 2019.

[62] M. Kacimi, M. Ziyad, and L. F. Liotta, “Cu on amorphous $AlPO_4$: preparation, characterization and catalytic activity in NO reduction by CO in presence of oxygen,” *Catal. Today*, vol. 241, pp. 151–158, 2015.

[63] J. Li, S. Wang, L. Zhou, G. Luo, and F. Wei, “NO reduction by CO over a Fe-based catalyst in FCC regenerator conditions,” *Chem. Eng. J.*, vol. 255, pp. 126–133, 2014.